Analysis of Generalized Mach–Zehnder Interferometers for Variable-Ratio Power Splitting and Optimized Switching

Neil S. Lagali, *Student Member, IEEE,* Mohammad R. Paiam, *Member, IEEE,* Robert I. MacDonald, *Senior Member, IEEE, Fellow, IEEE,* Kerstin Wörhoff, and Alfred Driessen, *Senior Member, IEEE*

***Abstract*—The nonideal integrated optical $N \times N$ generalized Mach–Zehnder interferometer (GMZI) employing multimode interference (MMI) couplers is analyzed using transfer matrix techniques. Deviations in the phase relations and the power splitting ratio of the MMI couplers are included in the theory, along with the effects of phase errors in the interferometer arms. The predictions of the theory are compared to the response of a 4 × 4 GMZI which has been fabricated. The device is operated as both a variable-ratio power splitter and a switch by compensating for the phase errors in the interferometer arms, but the performance is ultimately limited by the nonideal imaging in the MMI couplers. The practicality of these applications is investigated by performing a tolerance analysis for the operation of $1 \times N$ power splitters and switches for N up to 10.**

***Index Terms*—Multimode interference, optical couplers, optical switches, optical waveguide components.**

I. Introduction

MULTIMODE interference (MMI) couplers, based on the self-imaging effect [1] in slab waveguides, are key components in integrated optics. They function as efficient splitters and combiners of optical beams, while possessing a host of advantageous characteristics, such as low excess losses and low crosstalk [2], [3], accurate splitting ratios [4], [5], small device sizes [6], and good fabrication tolerances [7]. Furthermore, it has been shown that these features can be maintained independent of polarization, and for operation over a broad range of wavelengths [2], [7].

Owing to their superior performance, MMI couplers have been utilized as building blocks in more complex devices such as generalized (multiple-arm) Mach–Zehnder interferometer (GMZI) switches [8], [9]. The GMZI has subsequently been used in a number of wavelength division multiplexing (WDM) schemes, with applications in multifrequency lasers [10], flat-response wavelength demultiplexing [11], and wavelength-selective switching [12]. Recently, the functioning of the GMZI as an active variable-ratio power splitter has been described [13]. This device has interesting potential applications for emerging optical networks, where the nodes must optimally allocate and distribute signal power to numerous paths based on span length and/or changing demand.

Since the GMZI is an interferometric device, its performance depends upon the accuracy of the amplitudes and phases of multiple beams within the device. This places strict requirements on the performance of the constituent MMI couplers. In practice, errors in the phase relations and power splitting ratio of MMI couplers are present and can significantly degrade the performance and complicate the active control of devices based on the GMZI [9], [14], [15]. Furthermore, imperfect waveguide fabrication is known to cause additional phase errors [9], [16]. Since the arms of the GMZI are often relatively long to accommodate efficient phase shifting, the cumulative effects of these errors can be significant.

As the number and complexity of applications using the GMZI continues to expand, it becomes increasingly important to identify the limitations of these devices. In this paper, we quantify a number of nonideal performance parameters and determine their effect on the performance of the GMZI. In Section II, transfer matrix methods previously reported [9], [13] to describe the general power splitting capabilities of the GMZI are extended to include the effects of phase deviations and imbalance in power splitting ratio in the MMI couplers. The resulting model describes the characteristics of fabricated GMZI's and more accurately explains the difficulties in operating the GMZI. In Section III the general power splitting characteristics of a 4 × 4 GMZI which has been realized in silicon oxynitride (SiON) waveguide technology are compared to the behavior predicted by the model. Operation of the variable-ratio power splitter is described in Section IV, and a tolerance analysis of this device is performed. In Section V, the GMZI is shown to function as a $1 \times N$ switch by applying N sets of phase shifts to the N arms. Scalability of the switches is investigated and a tolerance analysis is performed, highlighting the strict requirements needed for realization of optimized switches using the GMZI configuration.

Manuscript received October 27, 1998; revised September 28, 1999. This work was supported by the Natural Science and Engineering Research Council of Canada, JDS Uniphase, Inc., and the MESA Research Institute, Lightwave Devices Group, University of Twente.

N. S. Lagali was with the Department of Electrical Engineering, University of Alberta, Edmonton, AB T6G 2G7 Canada. He is now with MESA-Faculty of Applied Physics, University of Twente, Enschede 7500 AE The Netherlands.

M. R. Paiam and and R. I. MacDonald are with JDS Uniphase, Inc., Nepean, Ont. K2C 3H1 Canada.

K. Wörhoff and A. Driessen are with MESA-Faculty of Applied Physics, University of Twente, Enschede 7500 AE The Netherlands.

Publisher Item Identifier S 0733-8724(99)09689-9.

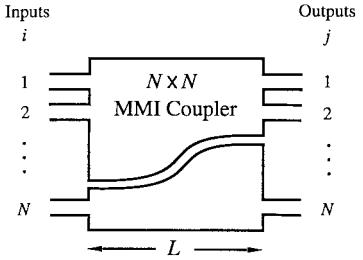

Fig. 1. Schematic diagram of a general $N \times N$ MMI coupler.

II. Theory of Non-Ideal GMZI Operation

A. Transfer Matrix of $N \times N$ MMI Coupler

Consider the $N \times N$ MMI coupler in Fig. 1. The coupler length L is given by [4]

$$L = \frac{3L_\pi}{N} \tag{1}$$

where L_π is the beat length of the coupler, defined as [3]

$$L_\pi = \frac{\pi}{\beta_0 - \beta_1} \tag{2}$$

where β_0 and β_1 are the propagation constants of the fundamental and first-order modes supported by the multimode region, respectively.

The phase associated with imaging an input i to an output j in an MMI coupler has been derived by Besse *et al.* [8], [17] and can be recast into a simpler form [18], yielding the relative phases φ_{ij}

$$\varphi_{ij} = -\frac{\pi}{2}(-1)^{i+j+N} + \frac{\pi}{4N} \cdot \left[i + j - i^2 - j^2 + (-1)^{i+j+N} \cdot \left(2ij - i - j + \frac{1}{2} \right) \right]. \tag{3}$$

Let us denote the transfer matrix for the $N \times N$ MMI by S_{coupler}. The element in row i and column j of this matrix, s_{ij}, is given by

$$s_{ij} = a_{ij} e^{J(\varphi_{ij} + \delta\varphi_{ij})} \tag{4}$$

where $J = \sqrt{-1}$, a_{ij} is the (real) field amplitude transfer coefficient from input i to output j, and $\delta\varphi_{ij}$ is the phase deviation of the image at output port j for an input into port i. In a lossless device, the optical power at the output ports is conserved, i.e.

$$\sum_{j=1}^{N} a_{ij}^2 = 1. \tag{5}$$

The output field distribution emerging from the MMI coupler is given by the following matrix equation:

$$\begin{bmatrix} E_1^{\text{out}} \\ E_2^{\text{out}} \\ \vdots \\ E_N^{\text{out}} \end{bmatrix} = S_{\text{coupler}} \begin{bmatrix} E_1^{\text{in}} \\ E_2^{\text{in}} \\ \vdots \\ E_N^{\text{in}} \end{bmatrix} \tag{6}$$

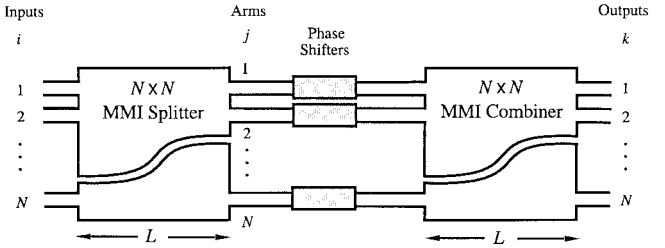

Fig. 2. General layout of an $N \times N$ generalized Mach–Zehnder interferometer. Identical $N \times N$ MMI couplers are used as splitter and combiner. The arms j are of the same length and have active phase shifting regions indicated by the shaded areas.

where E_i^{in} is the complex optical field amplitude at input port i and E_j^{out} is the optical field at output port j. The output intensities are $|E_j^{\text{out}}|^2$ and the imbalance in an output port (measured in dB units) is given by

$$\text{Imbalance} = 20 \cdot \log_{10} \left(\frac{a_{ij}}{a_{ij_{ref}}} \right) \tag{7}$$

where j_{ref} is a reference output port.

B. The GMZI Transfer Matrix

The basic layout of the $N \times N$ GMZI is shown in Fig. 2. The structure consists of three components: an $N \times N$ MMI splitter, an active phase shifting region with N arms and associated phase shifters, and an $N \times N$ MMI combiner. The phase shifters are indicated by shaded regions, and can be operated by applying a driving signal (voltage, current, etc.) to shift the phases of the light in the arms by virtue of any of a number of effects, such as the electrooptic or the thermooptic effect [19].

The transfer matrix of the GMZI consists of the matrix S_{splitter} with input ports i and output ports j and S_{combiner} with input ports j and output ports k. The active phase shifts are applied independently and simply shift the phase in a given arm j by an amount $\Delta\varphi_j$. The effect of phase errors in an arm caused by imperfect waveguide fabrication can be incorporated by introducing a phase error $\delta\varphi_j$ in the arm. The arms in a GMZI can therefore be described by the diagonal $N \times N$ transfer matrix

$$S_{\text{arms}} = \begin{bmatrix} e^{J(\Delta\varphi_1 + \delta\varphi_1)} & 0 & 0 & 0 \\ 0 & e^{J(\Delta\varphi_2 + \delta\varphi_2)} & 0 & 0 \\ 0 & 0 & \ddots & 0 \\ 0 & 0 & 0 & e^{J(\Delta\varphi_N + \delta\varphi_N)} \end{bmatrix}. \tag{8}$$

The total transfer matrix of the GMZI is then given by

$$T = S_{\text{combiner}} \cdot S_{\text{arms}} \cdot S_{\text{splitter}}. \tag{9}$$

C. Output Intensity Expressions

The elements of the transfer matrix T are denoted by t_{ik}, and are found by substituting (4) and (8) into (9)

$$t_{ik} = \sum_{j=1}^{N} a_{ij} a'_{jk} e^{J(\varphi_{ij} + \delta\varphi_{ij} + \Delta\varphi_j + \delta\varphi_j + \varphi_{jk} + \delta\varphi'_{jk})} \tag{10}$$

where the primed notation is used to distinguish the parameters of the MMI combiner from that of the splitter. In general the amplitude transfer coefficients will differ and phase deviations will vary from coupler to coupler and arm to arm. With a single input beam of optical intensity I_0 into port i, the intensity at an output port k is given by

$$I_k^{\text{out}} = |t_{ki}|^2 I_0 \tag{11}$$

where

$$|t_{ki}|^2 = \left(\sum_{j=1}^{N} a_{kj}^2 a_{ji}'^2\right) + 2\left[\sum_{p=1}^{N-1}\sum_{q=p+1}^{N} a_{kp}a_{pi}'a_{kq}a_{qi}' \cdot \cos[(\varphi_{ip}-\varphi_{iq}) + (\delta\varphi_{kp}-\delta\varphi_{kq}) + (\Delta\varphi_p - \Delta\varphi_q) + (\delta\varphi_p - \delta\varphi_q) + (\varphi_{pk}-\varphi_{qk}) + (\delta\varphi_{pi}' - \delta\varphi_{qi}')]\right] \tag{12}$$

and p and q refer to the internal arms j. Analytic expressions for the intensities at the various outputs in terms of the applied phase shifts, amplitude transfer coefficients, and phase deviations can be derived from (11). If these parameters are known, (11) contains N equations (one for each desired output power) and N unknowns (the applied phase shifts), and can be solved numerically to determine the phase shifts necessary to operate the GMZI as a generalized power splitter [13].

In practice, however, these parameters are not known, resulting in $2N^2 + 4N$ unknowns in (11). Determination of these parameters is exceedingly difficult unless the GMZI is physically separated into its splitter, arm, and combiner regions, which is impractical. The result is that the response of the GMZI to various applied phase shifts has not been predictable [9], [15], so optimization schemes or iterative methods are needed for the GMZI to be useful in optical switching or power splitting applications. Furthermore, the presence of imbalance and phase deviations in the MMI couplers and GMZI arms increase the crosstalk and reduce the extinction ratio attainable in the GMZI.

Improvement of waveguide fabrication technology can in principle solve these problems. For example, it is known that small variations in the width of MMI couplers results in imbalance and phase deviations among the output images [7]. Furthermore, imperfect waveguide fabrication can result in local variations in the waveguide width and core/cladding refractive indices, thereby introducing additional phase errors [16]. Since the arms of the GMZI consist of long, narrow, single-mode waveguides, the phase errors manifest themselves principally in the GMZI arms.

The analytic result (12) provides us with a model to determine the effects of imperfections on the performance of the GMZI. We now use this model to compare the predicted response of the GMZI under various nonideal conditions with the measured behavior of a 4 × 4 GMZI.

III. Characterization of a Fabricated GMZI

In an ideal GMZI, $\delta\varphi_{ij} \equiv 0$, $\delta\varphi_j \equiv 0$, and $a_{ij} = a_{ij}' \equiv 1/\sqrt{N}$, so (12) becomes

$$|t_{ki}|^2 = \frac{1}{N^2}\left\{N + 2\left[\sum_{p=1}^{N-1}\sum_{q=p+1}^{N} \cos[(\varphi_{ip}-\varphi_{iq}) + (\Delta\varphi_p - \Delta\varphi_q) + (\varphi_{pk}-\varphi_{qk})]\right]\right\}. \tag{13}$$

Choosing an arbitrary input port and setting all but one phase shift to zero, the power in the N output ports can be plotted as a function of a single phase shift. This is achieved experimentally by monitoring the optical intensity in the output ports as the power applied to a single phase shifter is continuously varied. In this manner, a "cross section" of the response of a fabricated GMZI is obtained, and can be compared to that of an ideal one. The deviation between the theoretical and the experimentally obtained functions indicate the degree to which phase deviations and imbalance are present in the fabricated device.

To illustrate this concept, we have fabricated a 4 × 4 GMZI in PECVD silicon oxynitride (SiON) waveguide technology [20]. A schematic diagram of this device is shown in Fig. 3. The rib waveguide cross section is given in the inset, and consists of a 1-μm thick core layer of SiON ($n = 1.559$) surrounded by upper and lower cladding regions of SiO_2 ($n = 1.459$), each 3 μm thick. The PECVD core and cladding layers were grown on thermally oxidized $\langle 100 \rangle$ oriented silicon wafers, and the waveguides were defined by a reactive ion etch (RIE). A 200 μm thick layer of chromium metal is deposited on top of each arm to serve as the thermooptic heater elements for phase shifting. The arms are separated by a lateral distance of 250 μm to increase the thermal isolation between them. The 4 × 4 MMI coupler dimensions are 16 × 259 μm.

Tunable laser light with a wavelength of 1550 nm is launched into an input port using a lensed single-mode fiber, and the light emerging from an output port is focused into a multimode fiber using microscope objectives. The fiber is terminated in a photodetector, and the output is electrically amplified and displayed by a multimeter. The thermooptic heaters are operated using four independent voltage sources.

An input port ($i = 2$) was arbitrarily chosen and the optical power in the output ports has been monitored while increasing the electrical power supplied to each single phase shifter while maintaining a zero applied power to the remaining three phase shifters. Four sets of sinusoidal curves are obtained. One such set is shown in Fig. 4, where the relative intensity in the output ports is plotted as a function of the electrical power applied to the phase shifter on arm $j = 4$ (arbitrarily chosen). The curved lines are fitted to the data points. The periodicity of the optical output is characteristic of an interferometer, and enables the calculation of the efficiency of the phase shifter. From Fig. 4, an applied electrical power of 204 mW results in a complete period or a 2π phase shift, for an efficiency of 32.5 mW / radian.

The experimental curves of Fig. 4 are reproduced for a single period in Fig. 5 (dashed lines) along with the theoretical

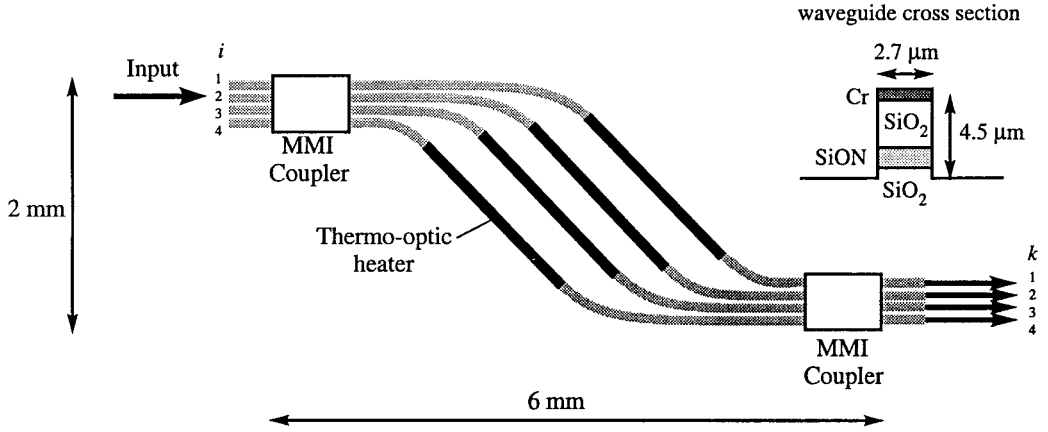

Fig. 3. General layout of the 4 × 4 GMZI which has been fabricated, showing the single-mode waveguide cross section (inset). The arms are separated by a distance of 250 μm and the thermooptic phase shifters are 3 mm in length.

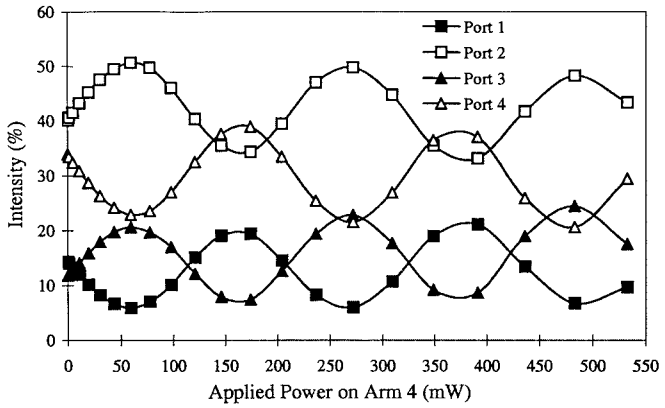

Fig. 4. Measured response from the output ports of a 4 × 4 GMZI. The optical intensities are expressed as a percentage of the total transmitted intensity and plotted as a function of the electrical power applied to the phase shifter on arm 4, and a zero applied power elsewhere. Input port $i = 2$ has been used.

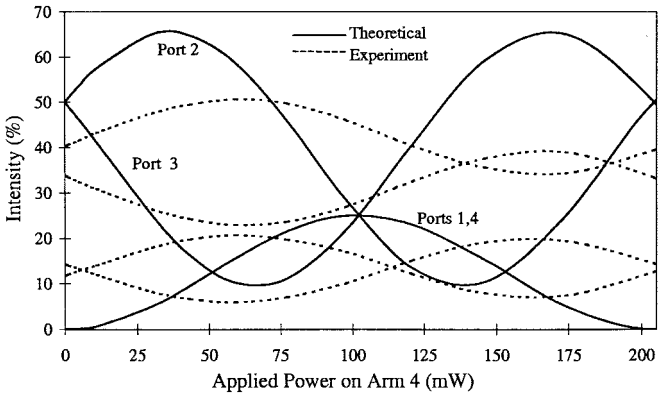

Fig. 5. The theoretical (solid line) response of a 4 × 4 GMZI over an applied phase shift of 2π is found from (13), and is superimposed on the experimental (dashed line) response of Fig. 4.

response of an ideal 4 × 4 GMZI (solid lines) calculated using (13). The fabricated device response is in general phase shifted, the amplitude of intensity variations is diminished, and the level about which the intensity varies sinusoidally is offset with respect to the ideal device. These results are evident from the form of (12), which contains terms which affect the amplitude, phase and offset of the sinusoidal variation of intensity with the applied phase shift.

We now use our model (12) to demonstrate how various nonideal effects result in our observed device response. First the model is used to determine the effects of imbalance and phase deviations in the MMI couplers. These effects have been introduced by first performing a modal propagation analysis (MPA) simulation [3] of the 4 × 4 MMI coupler using the waveguide design shown in Fig. 3. The result in Fig. 6 shows the maximum imbalance and phase deviation in the images for various MMI coupler lengths, using port 2 as a reference (arbitrary). A given level of imbalance and phase deviation can be associated with an equivalent length deviation, δL, which can arise from the finite resolution of the lithographic fabrication techniques used. For example, a deviation of ± 0.1 μm in the width of our MMI couplers results in an optimum imaging length variation of $\delta L = \pm 3$ μm. Values for $a, a', \delta\varphi$, and $\delta\varphi'$ are chosen randomly with upper limits corresponding to the imbalance and phase deviation levels for three different values of δL as shown in Fig. 6. These correspond to worst-case values from choosing each output port as a reference, and are introduced into (12), ensuring that the maximum imbalance and phase deviation are always present in at least one output port. The theoretical curve for an arbitrarily chosen output port $(k = 2)$ of the GMZI from Fig. 5 is then modified as shown in Fig. 7(a). Imbalance and phase deviations in the MMI couplers result in a slight shift in the phase of the theoretical response curve, and a slight change in both the offset level and the amplitude.

Next, we use the model to determine the effects of phase errors in the arms of the GMZI. Introducing random phase errors with various upper limits into (12), the theoretical curve for output port 2 from Fig. 5 is modified in the manner shown in Fig. 7(b). Phase errors in the arms of the GMZI significantly alter the phase, amplitude and offset level of the theoretical response. Observing the results of Fig. 7(b) and the experimental result in Fig. 5, there is strong evidence that phase errors are present in the fabricated device and are distributed approximately randomly among a range of values between 0 and 2π. These errors are approximated by random

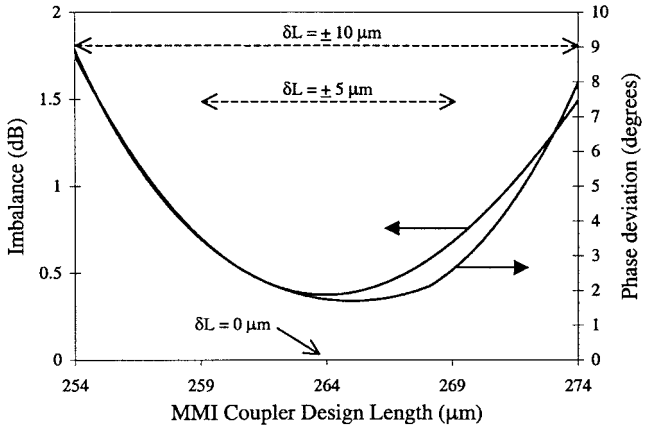

Fig. 6. MPA simulation results for our 4×4 MMI coupler, indicating the maximum imbalance and phase deviation that result when the MMI coupler length varies from the optimum imaging length $\delta L = 0$. Input port $i = 2$ and a reference port $j = 2$ have been used. Levels of imbalance and phase deviation (worst-case from all reference ports) corresponding to three different values of δL are chosen as benchmarks for a tolerance analysis of the GMZI.

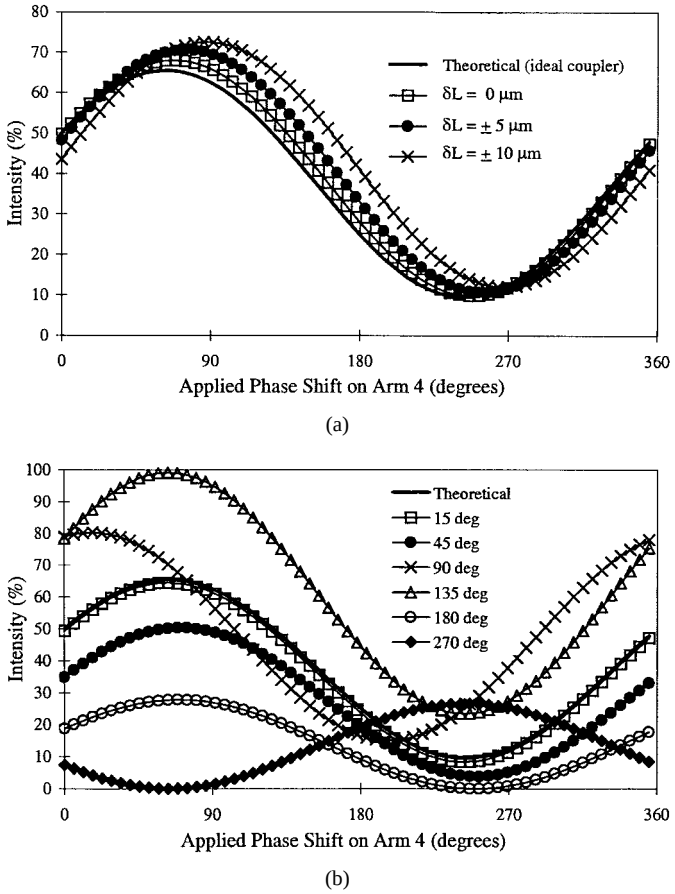

Fig. 7. Deviation of the theoretical response of port $k = 2$ from Fig. 5 calculated using (11) for various (a) equivalent length deviations in the MMI couplers, and (b) phase errors in the GMZI arms distributed randomly between 0° and various upper bounds.

values because material and waveguide parameters will vary locally from point to point in a given waveguide and arm to arm in a given device. If the magnitude of these random errors is limited to small fluctuations as shown in Fig. 7(b), the device response agrees reasonably well with the theory. In practice, the phase shifts applied to the arms can include

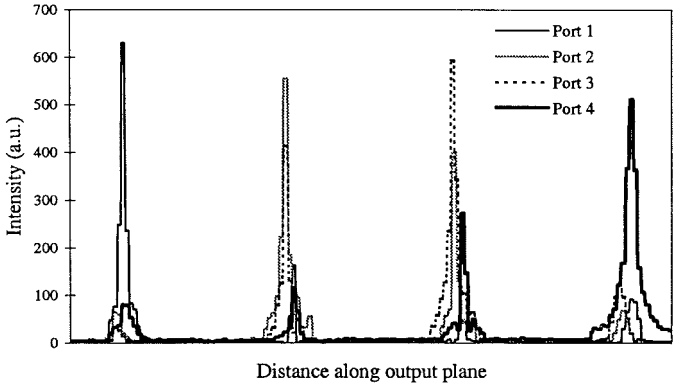

Fig. 8. Superimposed line scans of the four switch states of a 4×4 GMZI measured using an infrared camera. The phase shifter voltages were adjusted manually using an iterative technique to maximize the output light emerging from each port.

a bias component to compensate for the phase errors in the arms. Since the bias values needed are not known beforehand, we use the procedure outlined in the next section to determine these values experimentally.

IV. 4×4 Variable-Ratio Power Splitter

Using the 4×4 GMZI we have fabricated, we can demonstrate its operation as a variable-ratio power splitter. To compensate for the phase errors in the GMZI arms, the device is first brought into a switching state, where ideally all of the output light emerges from a single port. This has been done in our 4×4 device by adjusting the voltage applied to the four thermooptic phase shifters while the optical intensity emerging from the output ports was monitored using an infrared camera. The camera signal was sent to a computer, where image processing software was used to provide a line scan of the image. An iterative manual adjustment technique was used to bring the device to the four switch states. Line scans of these states are shown superimposed in Fig. 8. Though compensation of the phase errors in the arms is possible, the imbalance and phase deviations of the MMI couplers cannot in general be compensated by the applied phase shifts, resulting in increased crosstalk and nonuniformity in the switch states. The measured crosstalk values were typically -7 dB and a best result of -11 dB was obtained. Measured extinction ratios for all ports were between 15–18 dB.

The set of voltages corresponding to a switch state in our device were recorded, and the theoretical voltages needed to bring the switch into that state were subtracted from the set to arrive at a set of bias voltages. This set of bias voltages varied with each switch state, indicating imperfect imaging in the MMI couplers and partially uncompensated phase errors in the GMZI arms. Using the bias voltages and (13), the voltages necessary for a given variable-ratio power splitting state were calculated numerically. When these voltages were applied, the power splitting states varied slightly from the desired distribution, however, tuning of the voltages by a small amount from the predicted values often improved the splitting ratio. The reason for this is that (13) describes an ideal device and is therefore only an approximation. The results of this

TABLE I
SIMULATED TOLERANCES OF $N = 4$ VARIABLE-RATIO POWER SPLITTER FOR POWER SPLITTING RATIO (14), INCLUDING A $\pm 3\%$ INACCURACY IN THE APPLIED PHASE SHIFTS

MMI coupler deviation (Fig. 6 - worst case using all ports as a reference)			Upper limit for uncompensated phase error in interferometer arms (degrees)	Deviation in variable-ratio power splitting state (% of total output intensity) above (+) and below (-) desired value			
Equivalent δL	Imbalance (dB)	Phase Deviation (degrees)		Port $k = 1$	Port $k = 2$	Port $k = 3$	Port $k = 4$
Ideal coupler	0	0	0	- 0.04	- 0.37	+ 0.71	- 0.30
$\delta L = 0\ \mu m$	0.4	1.5	0	- 0.11	+ 1.17	+ 0.54	- 1.60
			5	+ 0.07	- 1.10	+ 3.49	- 2.46
$\delta L = \pm 5\ \mu m$	1.0	3.5	0	- 0.38	+ 1.34	- 3.17	- 4.13
			5	- 2.80	+ 4.57	+ 1.53	- 3.29
$\delta L = \pm 10\ \mu m$	2.0	9.0	0	- 1.33	+ 4.10	+ 8.13	- 10.91
			5	- 3.07	+ 6.08	+ 8.79	- 11.80

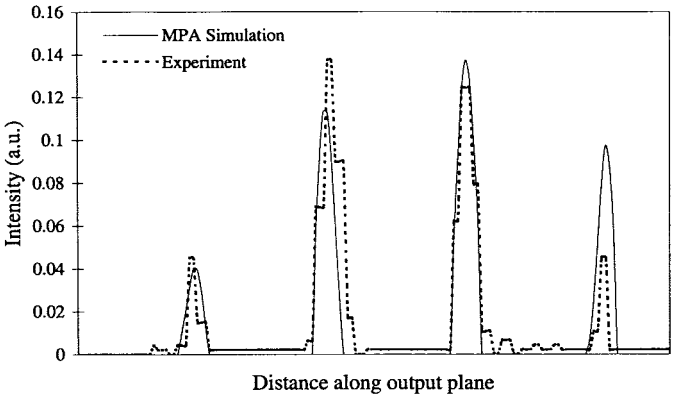

(a)

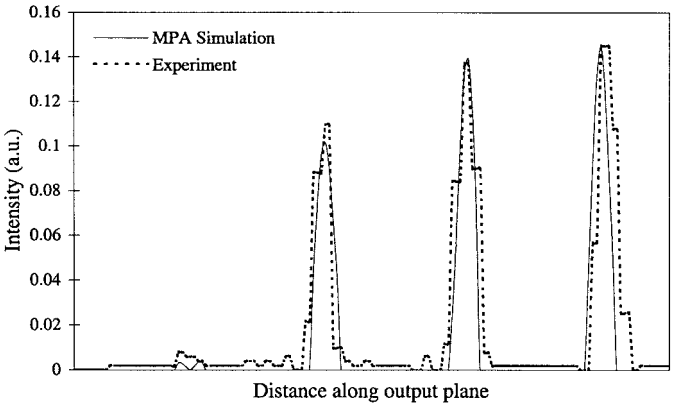

(b)

Fig. 9. Theoretical (solid line) and experimental (dashed line) output from a 4×4 variable-ratio power splitter for (a) the ratio given by (14), and (b) the ratio [0.00 0.33 0.33 0.34]. Theoretical results were found using the MPA technique [3].

method are shown for two power splitting ratios in Fig. 9. In Fig. 9(a), the best experimental result differs significantly from the theoretical prediction while the distribution in Fig. 9(b) closely matches the theoretical result. The power splitting ratio in Fig. 9(b) is one which can be accurately obtained in our fabricated GMZI, while the ratio in Fig. 9(a) cannot. This behavior is expected since the finite extinction ratio and crosstalk level in the fabricated device reduce the set of available power splitting ratios.

Table I summarizes the results of a tolerance analysis of variable-ratio power splitting with $N = 4$, using a power splitting state of

$$I_k^{\text{out}} = \begin{bmatrix} 0.10 \\ 0.30 \\ 0.40 \\ 0.20 \end{bmatrix} I_0 \tag{14}$$

corresponding to the state in Fig. 9(a). The required phase shifts are calculated from the theoretical result (13) which are used along with various values for nonidealities in (12), to calculate the resulting splitting ratio. The table lists the deviations of this ratio from the desired ratio given in (14). Various levels of imbalance and phase deviation in the MMI couplers have been introduced as an equivalent deviation in imaging length δL using the simulated results from Fig. 6. All values in the table include an inaccuracy component of $\pm 3\%$ of the value of the phase shift, which allows for the combined effects of a finite precision with which phase shifts can be applied, phase shift deviations due to wavelength variations in a 60-nm wavelength region around the center wavelength of 1550 nm, and fluctuations in the power applied to the phase shifters.

It is seen in Table I that a degradation in the power splitting ratio occurs as the imaging in the MMI couplers worsens. In this case, an acceptable level of deviation in the power splitting ratio is achieved if the equivalent deviation in imaging length of the 4×4 MMI couplers is kept below $\pm 5\ \mu$m. As the level of uncompensated phase errors in the GMZI arms increases from 0° to 5°, the effect on the deviation in the power splitting ratio is small when the MMI couplers are close to ideal, however, as the MMI coupler imaging degrades, the effects of errors in the arms become more significant. For the operation of the power splitter it is therefore of prime importance to ensure that the MMI couplers perform well.

To investigate larger devices, a similar tolerance analysis is performed for $N = 5$ up to $N = 10$ using an equal power splitting state in every case, i.e.,

$$I_k^{\text{out}} = \frac{I_0}{N} \tag{15}$$

where $k = 1, 2, \cdots, N$. The results are shown in Table II. To simulate the parameters of real devices, a maximum MMI coupler imbalance of ± 1.0 dB and phase deviation of $\pm 3.5^\circ$ are used for $N = 5, 6, 7$ and maximum imbalances and phase deviations of ± 2 dB and $\pm 9^\circ$, respectively, are used for $N = 8, 9, 10$. Low imbalance values such as these have been

TABLE II
SIMULATED TOLERANCES OF VARIABLE-RATIO POWER SPLITTER FOR $N = 5$ UP TO $N = 10$ FOR POWER SPLITTING RATIO (15), INCLUDING A $\pm 3\%$ INACCURACY IN THE APPLIED PHASE SHIFTS. THE IMBALANCE AND PHASE DEVIATION FOR $N = 5, 6, 7$ ARE ± 1.0 dB AND $\pm 3.5°$ AND FOR $N = 8, 9, 10$ THEY ARE ± 2.0 dB AND $\pm 9°$, RESPECTIVELY

N	Upper limit for uncompensated phase error in interferometer arms (degrees)	Deviation in equal power splitting state (% of total output intensity) above (+) and below (-) desired value									
		Output Port k									
		1	2	3	4	5	6	7	8	9	10
5	0	- 0.53	- 2.36	- 2.16	+ 3.26	+ 1.80					
	5	- 0.17	- 2.22	- 1.40	+ 2.52	+ 1.27					
6	0	+ 0.12	+ 0.99	- 1.31	+ 3.19	+ 0.72	- 3.71				
	5	+ 0.58	+ 2.30	- 1.95	+ 0.45	+ 0.24	- 1.62				
7	0	- 2.07	+ 2.35	- 1.11	- 0.98	- 2.12	+ 2.34	+ 1.58			
	5	- 0.95	+ 2.92	- 0.35	- 1.24	- 1.77	- 1.00	+ 2.39			
8	0	- 2.14	+ 1.15	- 2.15	+ 2.15	- 0.60	- 0.97	- 1.95	+ 4.52		
	5	- 2.06	+ 1.60	- 2.80	+ 1.84	- 0.70	- 1.00	+ 0.63	+ 2.49		
9	0	- 2.10	- 3.15	- 0.62	- 1.15	+ 1.61	+ 1.83	- 0.19	+ 1.29	+ 2.47	
	5	- 0.13	- 2.81	+ 1.26	- 2.80	+ 2.03	+ 0.21	+ 0.14	+ 0.95	+ 1.15	
10	0	- 2.74	- 0.05	- 1.38	- 3.66	- 1.65	- 1.75	+ 0.24	+ 0.19	+ 5.74	+ 5.05
	5	- 2.45	+ 1.87	- 2.84	- 4.94	- 0.03	- 2.30	+ 0.71	+ 0.25	+ 6.47	+ 3.26

measured in MMI couplers with large N [4], [5]. Table II also includes the phase shift inaccuracy values used in Table I.

The deviation in power splitting ratio is seen in Table II to increase slowly with increasing N. Maintaining a certain level of imbalance and phase deviations, however, becomes more difficult as N increases. This is because the tolerable length deviation δL required for a given level of imbalance and phase deviation in the MMI coupler shrinks as N increases. This effect is partially taken into account in the analysis by using larger imbalance and phase deviations for $N = 8, 9, 10$ than for $N = 5, 6, 7$. It is also seen in Table II that partially uncompensated phase errors in the GMZI arms have a small effect on the power splitting ratio N, sometimes improving the ratio due to partial compensation of the inaccuracies in the applied phase shifts.

The poor performance of the switching function in the GMZI shown in Fig. 8 is investigated by using our model (11) to perform a tolerance analysis for the switch. A similar procedure as for the power splitter is used, but replacing (14) by an arbitrarily chosen switch state. In this case, we use $I_k^{\text{out}} = I_0$ when $k = 4$, and $I_k^{\text{out}} = 0$ otherwise. The crosstalk for various MMI coupler deviations and inaccuracy allowances are shown in Table III, assuming the phase errors in the arms are fully compensated. Degradation in the imaging of the MMI couplers is seen to significantly increase crosstalk in the switch. If we add to this a small amount of uncompensated phase errors in the arms, the result is the poor performance we have measured.

From the trend in Table III, we observe that the imaging in the MMI couplers must first be improved to lower the crosstalk level. As the imaging approaches that of the ideal coupler, however, the sensitivity of the crosstalk to the accuracy of the phase shifting increases, indicating that simultaneous improvement of both the fabrication and control are needed to obtain good switch performance.

TABLE III
SIMULATED TOLERANCES FOR $N = 4$ GMZI SWITCH PERFORMANCE, ASSUMING FULLY COMPENSATED PHASE ERRORS IN THE ARMS, FOR VARIOUS LEVELS OF INACCURACY IN THE APPLIED PHASE SHIFTS

MMI coupler deviation (Equivalent δL)	Inaccuracy Allowance (± %)	Typical Crosstalk (dB)
Ideal coupler	0	- ∞
	1	- 44.8
	2	- 38.6
δL = 0 μm	0	- 30.0
	1	- 28.7
	2	- 27.0
δL = ± 5 μm	0	- 22.9
	1	- 22.4
	2	- 22.2
δL = ± 10 μm	0	- 14.1
	1	- 13.9
	2	- 13.8

V. OPTIMIZED GMZI SWITCHING

If for a given input port i the desired output distribution of the GMZI is set to a switch state and the idealized system of equations in (13) is numerically solved for the phase shifts, a set of switching phase shifts is obtained. By adding or subtracting a constant phase factor and using the modulo 2π operation, this set of phase shifts can be optimized, in the sense that the magnitude of the maximum difference among the phase shifts is minimized. Repeating this process for switch states corresponding to all N output ports, the resulting N sets of optimum switching phase shifts form the columns of a matrix, called the optimum switching matrix X. For a given input port i, the desired output port is selected by the column k, and the element in row j gives the phase shift that must be applied to arm j in order to route the light from input port i to output port k. Using a different input port amounts to interchanging the columns of the matrix X.

For example, the following optimum switching matrix is found for the 3×3 GMZI for $i = 1$:

$$X = \frac{\pi}{3}\begin{bmatrix} 1 & -1 & 1 \\ 1 & 1 & -1 \\ -1 & 1 & 1 \end{bmatrix} \tag{16}$$

which demonstrates that the $N = 3$ GMZI switch can be driven with phase shifters controlled by binary logic. If a 1×3

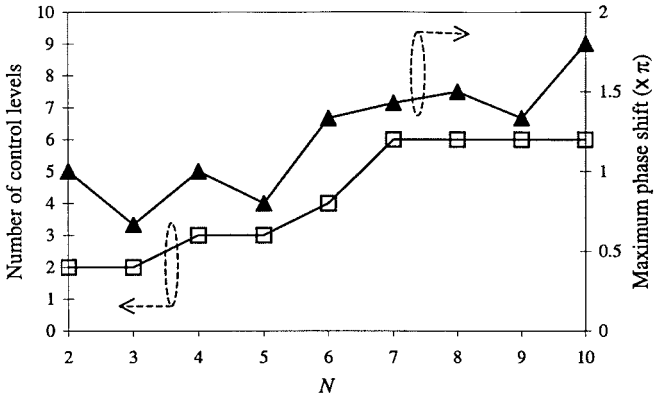

Fig. 10. Variation in the number of discrete phase shift control levels and the maximum phase shift required for optimized GMZI switch operation with the number of ports N.

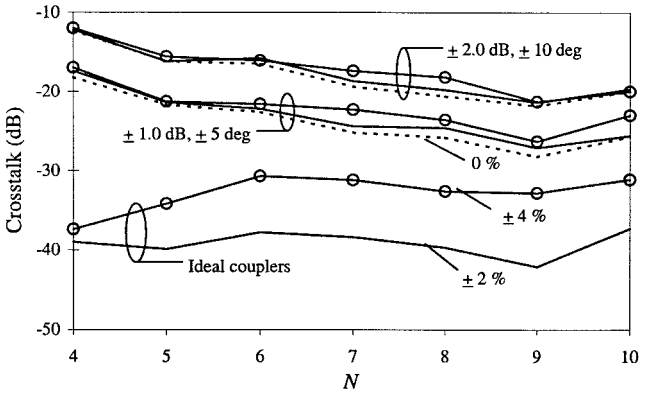

Fig. 11. Crosstalk in GMZI switches as a function of N for various MMI coupler performances and inaccuracy levels in the applied phase shifts. The dashed, solid, and circled lines are for inaccuracy levels of 0%, ±2%, and ±4%, respectively.

MMI coupler is used as the splitter, X is further simplified, though this is not true for a general value of N. The phase shifters in Fig. 2 can be designed such that the application of a voltage with magnitude of +V volts induces a phase shift of magnitude $2\pi/3$. The voltage levels 0 and +V therefore represent the digital logic levels 0 and 1, respectively.

Binary driving conditions are unique for the $N = 3$ GMZI switch. Generally, as N increases, the driving conditions for the phase shifters increase in complexity. For the $N = 5$ GMZI switch, however, the optimum switching matrix is given by the simple result

$$X = \frac{2\pi}{5}\begin{bmatrix} -1 & 0 & 1 & -1 & 1 \\ -1 & 1 & 0 & 1 & -1 \\ 1 & 1 & -1 & -1 & 0 \\ 1 & -1 & 1 & 0 & -1 \\ 0 & -1 & -1 & 1 & 1 \end{bmatrix} \tag{17}$$

which again demonstrates that the switch can in principle be driven with simple digital circuitry.

As N increases, the number of discrete phase shift (logic) levels increase, while the maximum phase shift magnitude required to operate the switch approaches 2π. A summary of the results obtained for switches with values of N up to ten are shown in Fig. 10. It should be mentioned that these results are idealizations, assuming the nonideal effects in a fabricated GMZI can be overcome. Even slight fabrication imperfections have been shown to result in nonideal behavior. While the GMZI can be used as a variable-ratio power splitter in these cases, the switching requirements are far more stringent. To exploit the symmetries in the GMZI for switching, it is imperative that the device response is as close as possible to the ideal response.

A tolerance analysis similar to the variable-ratio power splitter has been performed for GMZI switches for $N = 4$ up to $N = 10$, using a range of MMI coupler performances and inaccuracy allowances and assuming compensation of the phase errors in the GMZI arms. The results are shown in Fig. 11. Since optimum switching demands that the phase shifts are exact values, an additional inaccuracy resulting from fluctuations in the parameters of fabricated phase shifters such as resistance must also be included, and for this reason we have added an additional ±1% to the inaccuracy allowance in the analysis.

In Fig. 11 three levels of MMI coupler performance are used. If a certain level of MMI coupler performance can be maintained as N increases (usually resulting in tightened fabrication tolerances), the level of crosstalk will remain relatively constant. For perfect imaging in the MMI couplers (no imbalance or phase deviation) low crosstalk values are possible, but even slight inaccuracies in the applied phase shifts can degrade the crosstalk significantly. For example, a ±2% inaccuracy in the applied phase shifts increases the crosstalk from $-\infty$ (with no inaccuracy) to about −40 dB.

For a maximum imbalance of ±1.0 dB and phase deviation of ±5°, the crosstalk is limited to about −28 dB, while increasing these values to ±2.0 dB and ±10° limits the crosstalk to about −20 dB. Again as in Table III, the sensitivity of the crosstalk to the accuracy of the applied phase shifts decreases as the imaging in the MMI couplers degrades.

VI. Conclusion

We have developed a comprehensive model to simulate the behavior of nonideal $N \times N$ generalized Mach–Zehnder interferometers. By including effects such as variations in the MMI coupler imaging characteristics and phase errors in the arms, the predicted response of the nonideal GMZI resembles the response of a 4 × 4 GMZI we have fabricated. The GMZI can operate as both a variable-ratio power splitter and a switch, and a tolerance analysis has been performed for both functions, including errors in the MMI couplers and arms, and variations in operating parameters such as wavelength and stability in the applied phase shifting voltage. The variable-ratio power splitter can be operated even if the GMZI is nonideal and the splitting ratio remains stable and tolerant even for moderate values of N. The requirements for optimized switching using the GMZI, however, are far more stringent. The ultimate performance of these switches is determined by the imbalance and phase deviations in the MMI couplers. The switches provide crosstalk levels in the −20 to −30 dB range, and can only be improved with very accurate device fabrication and control methods.

REFERENCES

[1] O. Bryngdahl, "Image formation using self-imaging techniques," *J. Opt. Soc. Amer.*, vol. 63, pp. 416–419, 1973.

[2] E. C. M. Pennings, R. J. Deri, A. Scherer, R. Bhat, T. R. Hayes, N. C. Andreadakis, M. K. Smit, L. B. Soldano, and R. J. Hawkins, "Ultracompact, low-loss directional couplers on InP based on self-imaging by multimode interference," *Appl. Phys. Lett.*, vol. 59, pp. 1926–1928, 1991.

[3] L. B. Soldano, F. B. Veerman, M. K. Smit, B. H. Verbeek, A. H. Dubost, and E. C. M. Pennings, "Planar monomode optical couplers based on multimode interference effects," *J. Lightwave Technol.*, vol. 10, pp. 1843–1849, Dec. 1992.

[4] L. B. Soldano and E. C. M. Pennings, "Optical multi-mode interference devices based on self-imaging: Principles and applications (*Invited Paper*)," *J. Lightwave Technol.*, vol. 13, pp. 615–627, Apr. 1995.

[5] M. A. Fardad and M. Fallahi, "Sol-gel multimode interference power splitters," *IEEE Photon. Technol. Lett.*, vol. 11, pp. 697–699, June 1999.

[6] L. H. Spiekman, Y. S. Oei, E. G. Metaal, F. H. Groen, I. Moerman, and M. K. Smit, "Extremely small multimode interference couplers and ultrashort bends on InP by deep etching," *IEEE Photon. Technol. Lett.*, vol. 6, pp. 1008–1010, Aug. 1994.

[7] P. A. Besse, M. Bachmann, H. Melchior, L. B. Soldano, and M. K. Smit, "Optical bandwidth and fabrication tolerances of multimode interference couplers," *J. Lightwave Technol.*, vol. 12, pp. 1004–1009, June 1994.

[8] ——, "Phase relations in multi-mode interference couplers and their application to generalized integrated Mach-Zehnder optical switches," in *Proc. ECIO '93*, Apr. 1993, pp. 2.22–2.23.

[9] R. M. Jenkins, J. M. Heaton, D. R. Wight, J. T. Parker, J. C. H. Birbeck, G. W. Smith, and K. P. Hilton, "Novel $1 \times N$ and $N \times N$ integrated optical switches using self-imaging multimode GaAs/AlGaAs waveguides," *Appl. Phys. Lett.*, vol. 64, no. 6, pp. 684–686, Feb. 1994.

[10] M. R. Paiam and R. I. MacDonald, "A 12-channel phased-array wavelength multiplexer with multimode interference couplers," *IEEE Photon. Technol. Lett.*, vol. 10, pp. 241–243, Feb. 1998.

[11] C. K. Madsen, "A multiport frequency band selector with inherently low loss, flat passbands, and low crosstalk," *IEEE Photon. Technol. Lett.*, vol. 10, pp. 1766–1768, Dec. 1998.

[12] T. Aug.sson, "Theoretical investigation of a wavelength selective switch architecture based on a Bragg-grating-assisted MMIMI configuration," *IEEE Photon. Technol. Lett.*, vol. 11, pp. 839–841, July 1999.

[13] N. S. Lagali, M. R. Paiam, and R. I. MacDonald, "Theory of variable-ratio power splitters using multimode interference couplers," *IEEE Photon. Technol. Lett.*, vol. 11, pp. 665–667, June 1999.

[14] M. Bachmann, Ch. Nadler, P. A. Besse, and H. Melchior, "Compact Polarization-Insensitive Multi-Leg 1×4 Mach-Zehnder Switch in InGaAsP/InP," in *Proc. ECOC*, Firenze, Italy, 1994, pp. 519–522.

[15] P. A. Besse, M. Bachmann, Ch. Nadler, and H. Melchior, "The integrated prism interpretation of multileg Mach-Zehnder interferometers based on multimode interference couplers," *Opt. Quantum Electron.*, vol. 27, pp. 909–920, 1995.

[16] T. Goh, S. Suzuki, and A. Sugita, "Estimation of waveguide phase error in silica-based waveguides," *J. Lightwave Technol.*, vol. 15, no. 11, pp. 2107–2113, Nov. 1997.

[17] M.Bachmann, P.A. Besse, and H. Melchior, "General self-imagaing properties in $N \times N$ multimode interference couplers including phase relations," *Appl. Opt.*, vol. 33, no. 18, pp. 3905–3911, June 1994.

[18] M. R. Paiam and R. I. MacDonald, "Design of phased-array wavelength division multiplexers using multimode interference couplers," *Appl. Opt.*, vol. 36, no. 21, pp. 5097–5108, July 1997.

[19] H. Nishihara, M. Haruna, and T. Suhara, *Optical Integrated Circuits*. New York: McGraw-Hill, 1989, ch. 5.

[20] N. S. Lagali, M. R. Paiam, R. I. MacDonald, K. Wörhoff, and A. Driessen, "4×4 variable-ratio integrated optical power splitter," in *Proc. ECIO*, Torino, Italy, Apr. 1999, Postdeadline papers, pp. 9–12.

Neil S. Lagali (S'99), photograph and biography not available at the time of publication.

Mohammad R. Paiam (M'97), photograph and biography not available at the time of publication.

Robert I. MacDonald (SM'87), photograph and biography not available at the time of publication.

Kerstin Wörhoff, photograph and biography not available at the time of publication.

Alfred Driessen (M'93–SM'95), photograph and biography not available at the time of publication.